

# New nanostructured $\text{Al}_2\text{Zr}_{2-x}\text{V}_x\text{O}_7$ pyrochlore: structural, electrical and dielectric behavior evaluation for high frequency devices fabrication

S. MUMTAZ<sup>a</sup>, M. FAROOQ WARSI<sup>b</sup>, M. NAEEM ASHIQ<sup>a</sup>, N. KARAMAT<sup>a</sup>, I. SHAKIR<sup>c,\*</sup>

<sup>a</sup>Institute of Chemical Sciences, Bahuddin Zakaryia University, Multan, Pakistan

<sup>b</sup>Department of Chemistry, Baghdad-Ul-Jadeed Campus, The Islamia University of Bahawalpur, Bahawalpur-63100, Pakistan

<sup>c</sup>Deanship of scientific research, College of Engineering, PO Box 800, King Saud University, Riyadh 11421, Saudi Arabia

Nanostructured  $\text{Al}_2\text{Zr}_2\text{O}_7$  and its vanadium Substituted derivatives  $\text{Al}_2\text{Zr}_{2-x}\text{V}_x\text{O}_7$  ( $x=0, 0.25, 0.50, 0.75, 1.0$ ) were prepared by the sol-gel auto-combustion method. The pyrochlore  $\text{Al}_2\text{Zr}_{2-x}\text{V}_x\text{O}_7$  nanoparticles were characterized by energy dispersive X-ray spectroscopy (EDX), Fourier-transformed infrared (FTIR) spectroscopy, X-ray diffraction (XRD). The electrical resistivity was measured at varied temperature in the range of 300 to 675 K. The maximum electrical resistivity ( $119.88 \times 10^8$  ohm cm) was observed by  $\text{Al}_2\text{ZrVO}_7$  ( $x=1.00$ ) while  $\text{Al}_2\text{Zr}_2\text{O}_7$  ( $x=0.00$ ) exhibited the minimum resistivity ( $56.85 \times 10^8$  ohm cm) at the same temperature. The dielectric behavior was measured at room temperature. All the dielectric parameters were found to decrease with increase in vanadium contents. The increase in electrical resistivity while decrease in dielectric behavior on substitution suggested that these materials may find potential applications in microwave devices as such devices required highly resistive materials.

(Received January 14, 2015; accepted March 19, 2015)

**Keywords:** Pyrochlore, Nanostructures, Electrical resistivity, Dielectric properties

## 1. Introduction

Nanostructured materials are being paid significant consideration since last few decades because of their quite distinct behavior from their bulk counter parts [1-4]. For example, the well known example is the presence of surface plasmon band in metal nanoparticles which is usually absent in bulk metals [5]. Among various types of nanomaterials, the metal oxides nanostructures are an important class of advanced smart functional materials [6, 7]. There are further several classes of metal oxides, for example the perovskites, spinels, pyrochlores etc. Every class of metal oxides has its significance due to certain technological importance and applications in other related areas [8, 9]. The perovskites ( $\text{ABO}_3$ ) are mostly studied for their applications as cathode materials (for solid oxide fuel cells applications), sensors, catalysts, ferroelectrics etc [10]. The spinels are mostly utilized in microwave devices, telecommunications and recording media/data storage technology [11-15]. Pyrochlores are the metal oxides with general formula  $\text{A}_2\text{B}_2\text{O}_7$  where A usually trivalent cation and B is tetravalent [16]. In the structure of pyrochlore compound  $\text{A}^{3+}$  ion is placed at the 16c site,  $\text{B}^{4+}$  cation may be from 3d,4d and 5d block elements like  $\text{Zr}^{4+}$ ,  $\text{Sn}^{4+}$  etc and is at 16d site [3, 6] and  $\text{O}^{2-}$  ion may be at 48f or 8a sites. Since a vacant site is also present at 8b site for ordered pyrochlore structure. Pyrochlore are being given special interest due to their versatile applications such as nuclear waste storage materials, electrolytes in solid oxide

fuel cell and oxygen sensors [17, 18]. Further these materials may also have their applications in various technologies due to their wide range of electrical behavior ranging from insulating to metallic behavior. Pyrochlore oxides are also used in thermistors, capacitors, switching technology, resistors and microwave communications. Among several pyrochlore oxides, the  $\text{M}_2\text{Zr}_2\text{O}_7$  for example lanthanide zirconates ( $\text{Ln}_2\text{Zr}_2\text{O}_7$ ),  $\text{La}_2(\text{Zr}_x\text{Ce}_{1-x})\text{O}_7$ ,  $\text{Y}_2\text{Ti}_2\text{O}_7$  and  $\text{Ce}_2\text{Zr}_2\text{O}_{8-x}$  etc are the zirconate pyrochlore oxides extensively studied for various applications such as solid oxide fuel cells [19], catalytic applications[20], gas sensors and high frequency electronic devices such as oscillator, resonators and frequency filters [21-23].

In the present work we have selected new composition of zirconate ( $\text{Al}_2\text{Zr}_2\text{O}_7$ ) pyrochlore material. The effect of vanadium substitution on the electrical and dielectric properties has also been investigated. The main aim of the present work is to enhance the electrical resistivity of the materials that is required for applications in high frequency microwave devices.

## 2. Experimental

### 2.1 Chemicals

Chemicals used for the synthesis of  $\text{Al}_2\text{Zr}_{2-x}\text{V}_x\text{O}_7$  oxides nanoparticles were Vanadium oxide ( $\text{V}_2\text{O}_5$ , 99%,

Sigma-Aldrich), Aluminium nitrate ( $\text{Al}(\text{NO}_3)_3 \cdot 9\text{H}_2\text{O}$ , 98.5%, Merck), Zirconium oxychloride ( $\text{ZrOCl}_2 \cdot 8\text{H}_2\text{O}$ , 98%, Hopkin and William), Ethylene glycol (99%, Fluka), Aqueous ammonia solution (35%, Fischer Analar). The chemicals were of analytical grade and were used as such without further treatment.

## 2.2 Synthesis of $\text{Al}_2\text{Zr}_{2-x}\text{V}_x\text{O}_7$ nanoparticles

The chemical sol gel method was used to synthesize the nanoparticles of  $\text{Al}_2\text{Zr}_{2-x}\text{V}_x\text{O}_7$  having various compositions i.e.  $x = 0.00, 0.25, 0.50, 0.75, 1.0$  [24, 25]. Solutions of required molarities of the metal salts were prepared in deionized water. The vanadium oxide was first dissolved in 5 mL of HCl and then volume make up with deionized water. Then solutions were mixed in beaker and stirred on hot plate. The ethylene glycol was added in the reaction mixture as chelating agent and the ratio between metal solution and ethylene glycol was kept 1:1.5. After that the pH of the solution was maintained at 7 by adding 2M ammonia solution. The mixture was then heated at  $80^\circ\text{C}$  and after evaporation it was converted into gel. The gel was then burnt at  $300^\circ\text{C}$  and finally annealed the powder at  $850^\circ\text{C}$  in a box furnace (Vulcan A550) for 8 hours.

## 2.3 Characterization

The phase formation of the synthesized materials was confirmed by X-ray diffraction analysis by using X-ray Diffractometer (Philips X' Pert PRO 3040/60) which uses Cu  $K\alpha$  as radiation source. The FTIR analysis was also carried out to confirm the formation of zirconates using (Nexus 470) spectrometer. The composition of the synthesized materials was confirmed by EDX analysis using Jeol JSM-6490A electron microscope (Fig. 1 and Table 1). The DC electrical resistivity was measured by two point probe method using (Kiethly source meter 2400) and UT55 multimeter. The dielectric parameters such as dielectric constant  $\epsilon$ , dielectric loss  $\epsilon''$  and tanloss were measured by using (Wayne Ker WK6500B) LCR meter.

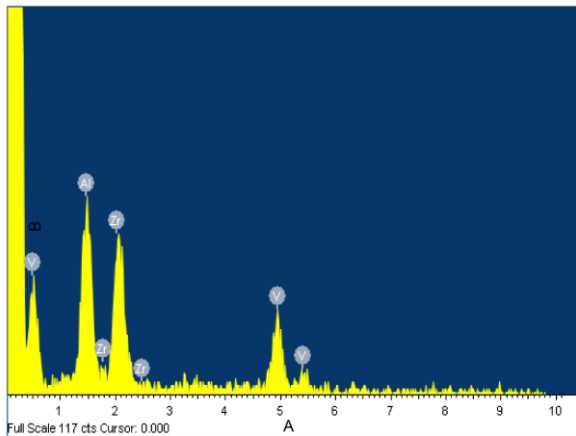


Fig. 1. EDX spectrograph of  $\text{Al}_2\text{Zr}_{2-x}\text{V}_x\text{O}_7$  ( $x=0.5$ ) nanoparticles.

Table 1. Elemental compositions of  $\text{Al}_2\text{Zr}_{2-x}\text{V}_x\text{O}_7$  nanoparticles as determined by EDX analysis.

Elements (atomic %)	x= 0	x= 0.25	x= 0.50	x = 0.75	x= 1.0
Al	45.61	44.29	42.18	43.79	46.70
Zr	43.79	26.91	22.04	6.86	6.81
V	8.15	10.47	11.92	30.91	32.35

## 2.4 Calculations

The crystallite size (D), lattice constant, cell volume and X-ray density was calculated from the XRD data using the following equations.

$$d = \frac{K\lambda}{\beta \cos \theta} \quad (1)$$

$$a = d (h^2 + k^2 + l^2)^{1/2} \quad (2)$$

$$V = a^3 \quad (3)$$

$$\rho_{\text{x-ray}} = ZM/N_A V \quad (4)$$

Where " $\lambda$ " is the X-ray wavelength and is equal to  $1.542\text{\AA}$ , " $\beta$ " is full width at half maxima, " $\theta$ " is the Bragg's angle and K is the constant and its value is 0.9,  $h, k, l$  are miller indices, " $Z$ " is the number of formula units in a unit cell, " $M$ " is molecular mass of the sample and  $N_A$  is the Avogadro's number.

The electrical resistivity of the samples was calculated by the following equation.

$$\rho = \frac{RA}{l} \quad (5)$$

Where " $\rho$ " is resistivity, " $R$ " is the resistance of the sample, " $A$ " and " $l$ " are the area and length of the sample pallet, respectively.

The dielectric constant was calculated by the following equations.

$$\epsilon' = \frac{Cd}{\epsilon_0 A} \quad (6)$$

Where  $A$  is the area of pellet,  $\epsilon_0$  is the constant of permittivity of free space,  $C$  is capacitance of the pellet (in farad) and  $d$  is the thickness of the pellet. The dielectric loss ( $\epsilon''$ ) and  $\tan\delta$  were calculated by the following equations.

$$\epsilon' = \epsilon'' \tan \delta \quad (7)$$

$$\tan \delta = \frac{1}{2\pi f R_p C_p} \quad (8)$$

Where  $R_p$  is equivalent parallel resistance  $C_p$  is equivalent parallel capacitance and  $f$  is the frequency [26, 27].

### 3. Results and discussion

#### 3.1 EDX analysis

The typical EDX graph for  $Al_2Zr_{0.5}V_{0.5}O_7$  is shown in Fig. 1.0 and all other graphs are given in electronic supplementary information (Fig. S1 to S4). All the peaks are labeled for the elements present in the materials. The atomic %age of each element as determined by EDX analysis in all compositions are given in Table 1. It is clear from the table that the experimental data obtained was found in good agreement with the theoretical calculations.

#### 3.2 XRD analysis

The XRD patterns for all samples are shown in Fig. 2.0. All the peaks were matched with the standard pattern ICDD-00-008-0221 which confirmed that all the samples have single phase structure with miller indices 222, 400, 440 and 622 at  $2\theta = 28.6, 34.1, 49.2$  and  $57.3^\circ$  respectively (Fig. 2.0). However at higher concentration of substitution a small peak appeared for the vanadium oxide impurity. It is due to less solubility of vanadium than that of zirconate. Various parameters like lattice constant, cell volume, x-ray density and crystalline size were calculated from the XRD data using equation 1-4 (Table 2).

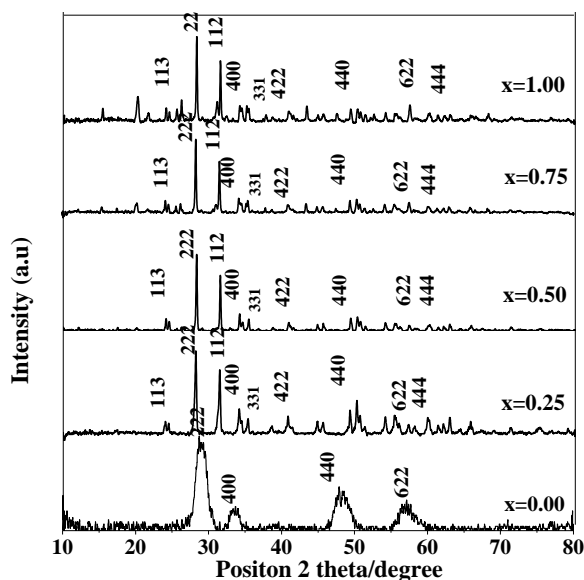


Fig. 2. XRD Patterns of " $Al_2Zr_{2-x}V_xO_7$ " nanoparticles annealed at  $700^\circ C$ .

The crystallinity of the samples was increased on the substitution as indicated by sharpness of the peaks in the XRD pattern. The crystallites size of vanadium doped aluminium zirconates was found in the range of 6 to 42 nm that is required for many applications such as photo-

catalysis etc [28]. The cell volume (V) and lattice constant (a) of vanadium doped  $Al_2Zr_{2-x}O_7$  were found to decrease with increased dopant contents (Table 2.0). This decreased in cell parameters were due to smaller ionic radius of vanadium ( $0.59\text{\AA}$ ) as compared to zirconium ( $0.80\text{\AA}$ ). The X-ray density of vanadium doped aluminium zirconate decreased with increased vanadium content which is due to higher molar mass of vanadium as compared to zirconium. These results are found in compatible with already reported results for similar compounds [8, 9].

Table 2. Lattice constants (a, b and c), cell volume, x-ray density, porosity and crystallite size of  $Al_2Zr_{2-x}V_xO_7$  nanoparticles.

Parameters	x=0	x=0.25	x=0.50	x=0.75	x=1.0
Lattice constant $a/\text{\AA}\pm 0.01$	10.74	10.33	10.08	9.95	9.48
Cell Volume/ $\text{\AA}^3\pm 0.01$	1241	1102	1023	986	853
X-ray Density/ $\text{gcm}^{-3}$ $\pm 0.01$	3.72	4.07	4.25	4.28	4.79
Crystallite Size/nm	6.35	39.20	42.21	39.87	38.40

#### 3.3 FTIR analysis

The FTIR spectrum for  $Al_2Zr_{2-x}V_xO_7$  ( $x=0.50$ ) is shown in the supplementary information (Fig. S5). The vibration bands in synthesized material were observed at  $1006.8, 562.0, 465.2, 441.3, 418.3$  and  $401.1\text{ cm}^{-1}$ . The absorption peaks at  $1006$  and  $562\text{ cm}^{-1}$  are due to stretching vibrations of  $ZrO_2$  [29]. Similarly the absorption peaks at  $465\text{ cm}^{-1}$  of pyrochlore structure which belongs to vibrational mode of  $MO_8$  and  $ZrO_6$  [30]. The IR bands between  $400$  to  $420\text{ cm}^{-1}$  confirmed fluorite structure [31, 32].

#### 3.4 DC-Electrical resistivity

The temperature dependence electrical resistivity which was calculated from the equation (5) in the temperature range of  $300-675\text{ K}$  is shown in the Fig. 3. The behavior of electrical resistivity shows two different regions. In 1<sup>st</sup> region (Region I) the electrical resistivity increases with increase in temperature while after a certain temperature ( $373\text{ K}$ ) the electrical resistivity decreases with the increase in temperature (Region II). Region I shows metallic behavior while Region II is due to semiconductor behavior. The temperature at which maximum value of electrical resistivity ( $\rho$ ) was observed is called metal to semiconductor transition temperature ( $T_{M-S}$ ). The value of  $T_{M-S}$  shifted towards higher value with the vanadium substitution. There are various factors which are responsible for such behavior like phase transition, cation migration, cations reordering, presence of impurities and structure disorder. So here, the transition temperature  $T_{M-S}$  is due to the presence of impurity and as

well as phase transition which is also confirmed by the XRD analysis.

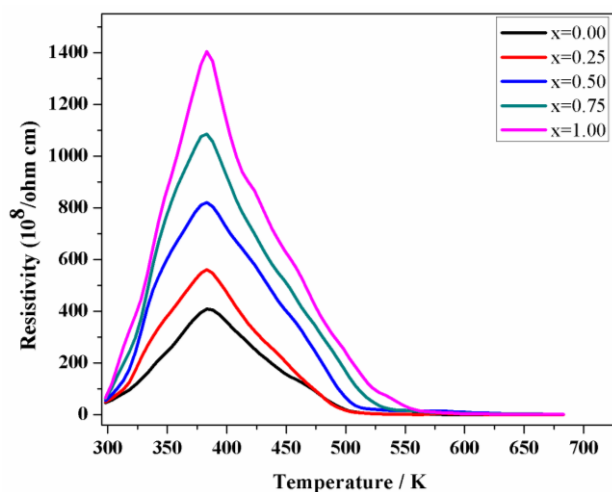


Fig. 3. Effect of temperature on resistivity of " $\text{Al}_2\text{Zr}_{2-x}\text{V}_x\text{O}_7$ " nanoparticles.

The room temperature (300K) resistivity increased with the increase in substituent (vanadium) concentration as shown in Fig. 4. In most ordered and disordered pyrochlore (fluorite) system, the ionic conduction is carried out by oxygen vacancies hopping between 48f sites [33, 34]. The radius ratio  $r_A/r_B$  and lattice constant can affect the conduction mechanism [35]. The decrease in the radius ratio tends to produce disorder and also oxygen vacancy which enables easy hopping of oxide ions due to equivalent anionic sites creation. So here in present work, the introducing of vanadium has small ionic radius, that's why similar behavior is observed. Similarly the decrease in lattice constant also decrease the lattice free space so easily free ions are not available for the conduction process and the room temperature resistivity increased with the increasing substitution concentration (Fig. 4) [36].

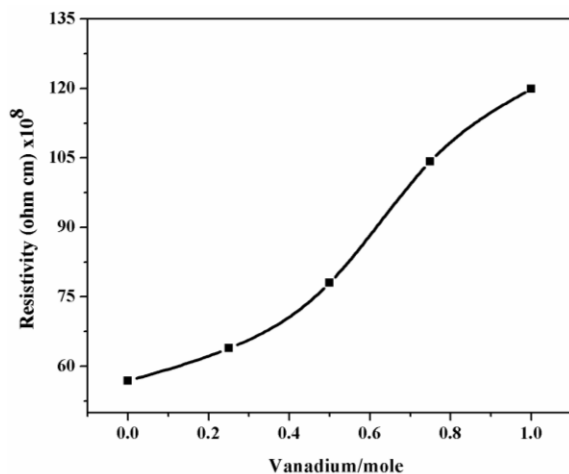


Fig. 4. Effect of Vanadium content on resistivity of " $\text{Al}_2\text{Zr}_{2-x}\text{V}_x\text{O}_7$ " nanoparticles at 300 K.

### 3.5 Dielectric parameters

The dielectric parameters like dielectric constant, dielectric loss and dielectric loss factor were measured at 298 K. The effect of vanadium contents on dielectric constant, tan loss and dielectric loss at 1 GHz frequency are shown Figs. 5-7, respectively. From Fig. 5 it is clear that with the increase of vanadium substitution the dielectric constant decreases. It is due to less ionic radius of vanadium which produced less polarization. The dielectric properties are greatly influenced by the incorporation at B-site as compared with the substitution at A-site [37].

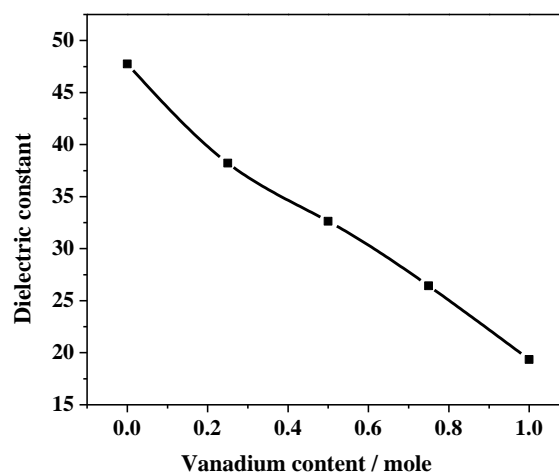


Fig. 5. Effect of Vanadium content on dielectric constant of " $\text{Al}_2\text{Zr}_{2-x}\text{V}_x\text{O}_7$ " nanoparticles at 1 GHz frequency.

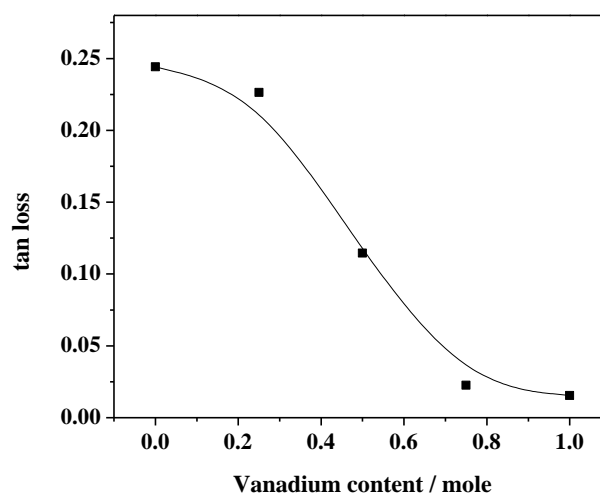


Fig. 6. Effect of Vanadium content on tan loss of " $\text{Al}_2\text{Zr}_{2-x}\text{V}_x\text{O}_7$ " nanoparticles at 1 GHz frequency.

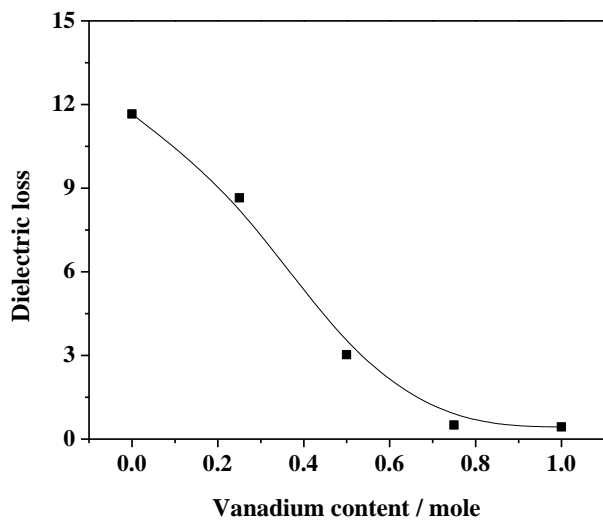


Fig. 7. Effect of Vanadium content on dielectric loss of " $Al_2Zr_{2-x}V_xO_7$ " nanoparticles at 1 GHz frequency.

Similarly the dielectric loss and tan loss factor also decreased with the increasing substituent concentration due to increasing trend of grain size. Since as grain size increases, the reduction in the grain boundaries per unit volume would occurred, which results in decreasing effect of dielectric loss of material [6].

So increasing trend of electrical resistivity and decreasing trend of dielectric properties would results that material is suitable for the electronic devices such as resonators, oscillators and frequency filters etc.

#### 4. Conclusions

The new substituted  $Al_2Zr_{2-x}V_xO_7$  nanoparticles in the range of 6-42 nm were prepared by cheap economic route i.e. chemical sol-gel method. The prepared nanoparticles were successfully characterized by EDX, FTIR and XRD. The electrical resistivity measurements showed that, about 2 fold DC-electrical resistivity was enhanced by replacement of Zr with V in  $Al_2Zr_{2-x}V_xO_7$ . The high resistivity materials may be used in microwave devices fabrications. Both electrical and dielectric parameters suggest the various potential applications of new  $Al_2Zr_{2-x}V_xO_7$  pyrochlore materials.

#### Acknowledgement

Dr. Imran Shakir would like to extend their sincere appreciation to the Deanship of Scientific Research at the King Saudi University for its funding of this research through the Research Group Project no RGP-VPP-312.

#### References

- [1] M. F. Warsi, R. W. Adams, S. B. Duckett, V. Chechik, *Chemical Communications*, **46**, 451 (2010).

- [2] Z. Li, Y. Wang, Q. Yu, *J. of Materi Eng and Perform*, **19**, 252 (2010).
- [3] K. R. Patil, Y. K. Hwang, D.-K. Kim, J.-S. Chang, S.-E. Park, *Bull. Korean Chem. Soc.*, **26**, 1025 (2005).
- [4] A. Sharifnabi, B. Eftekhari Yekta, M. Fathi, M. Hossainipour, *J Sol-Gel Sci Technol*, 1-12 (2014).
- [5] M. F. Warsi, V. Chechik, *Physical Chemistry Chemical Physics*, **13**, 9812 (2011).
- [6] G. E. Brown, V. E. Henrich, W. H. Casey, D. L. Clark, C. Eggleston, A. Felmy, D. W. Goodman, M. Grätzel, G. Maciel, M. I. McCarthy, K. H. Nealsen, D. A. Sverjensky, M. F. Toney, J. M. Zachara, *Chemical Reviews*, **99**, (1998).
- [7] S. Surnev, A. Fortunelli, F. P. Netzer, *Chemical Reviews*, **113**, 4314 (2012).
- [8] A. Mahmood, M. F. Warsi, M. N. Ashiq, M. Sher, *Materials Research Bulletin*, **47**, 4197 (2012).
- [9] A. Mahmood, M. F. Warsi, M. N. Ashiq, M. Ishaq, *Journal of Magnetism and Magnetic Materials*, **327**, 64 (2013).
- [10] Y.-P. Fu, H.-C. Wang, S.-H. Hu, K.-W. Tay, *Ceramics International*, **37**, 2127 (2011).
- [11] Y. Hwang, *Materials Letters*, **60**, 3277 (2006).
- [12] H.-C. Shin, S.-C. Choi, K.-D. Jung, S.-H. Han, *Chemistry of Materials*, **13**, 1238 (2001).
- [13] J. Song, L. Wang, N. Xu, Q. Zhang, *Journal of Materials Science & Technology*, **26**, 787 (2010).
- [14] S. Elangovan, S. Balagopal, M. Timper, I. Bay, D. Larsen, J. Hartvigsen, *J. of Materi Eng and Perform*, **13**, 265 (2004).
- [15] Y. I. Kim, H. Kang, D. Kim, C. S. Lee, *Bull. Korean Chem. Soc.*, **24**, 593 (2003).
- [16] B. Huang, Y. Liu, Y. Lu, H. Gao, H. Chen, *J Mater Sci: Mater Electron*, **24**, 2785 (2013).
- [17] A. F. Qasrawi, B. H. Kmail, A. Mergen, *Ceramics International*, **38**, 4181 (2012).
- [18] F. Xiang, H. Wang, M. Zhang, X. Sun, X. Yao, *Ceramics International*, **34**, 925 (2008).
- [19] D. J. L. Brett, A. Atkinson, N. P. Brandon, S. J. Skinner, *Chemical Society Reviews*, **37**, 1568 (2008).
- [20] M. P. van Dijk, J. H. H. ter Maat, G. Roelofs, H. Bosch, G. M. H. van de Velde, P. J. Gellings, A. J. Burggraaf, *Materials Research Bulletin*, **19**, 1149 (1984).
- [21] M. Kumar, M. A. Kulandainathan, I. A. Raj, R. Chandrasekaran, R. Pattabiraman, *Materials Chemistry and Physics*, **92**, 303 (2005).
- [22] A. Banerji, B. P. Mandal, T. N. Sairam, A. K. Tyagi, *Solid State Communications*, **151**, 321 (2011).
- [23] J. Wang, F. Zhang, J. Lian, R. C. Ewing, U. Becker, *Acta Materialia*, **59**, 1607 (2011).
- [24] A. Kahoul, P. Nkeng, A. Hammouche, F. Naamoune, G. Poillierat, *Journal of Solid State Chemistry*, **161**, 379 (2001).
- [25] C. L. Carnes, K. J. Klabunde, *Journal of Molecular Catalysis A: Chemical*, **194**, 227 (2003).
- [26] M. J. Iqbal, M. N. Ashiq, P. H. Gomez, *Journal of Alloys and Compounds*, **478**, 736 (2009).
- [27] M. N. Ashiq, M. J. Iqbal, I. H. Gul, *Journal of Alloys and Compounds*, **487**, 341 (2009).

- [28] Y. Tong, P. Xue, F. Jian, L. Lu, X. Wang, X. Yang, *Materials Science and Engineering: B*, **150**, 194 (2008).
- [29] H. R. Sahu, G. R. Rao, *Bulletin of Materials Science*, **23**, 349 (2000).
- [30] M. Kumar, M. A. Kulandainathan, I. A. Raj, R. Chandrasekaran, R. Pattabiraman, *Materials Chemistry and Physics*, **92**, 295 (2005).
- [31] N. A. Dhas, K. C. Patil, *Journal of Materials Chemistry*, **3**, 1289 (1993).
- [32] H. Ranjan Sahu, G. Ranga Rao, *Bull Mater Sci*, **23**, 349 (2000).
- [33] M. Pirzada, R. W. Grimes, L. Minervini, J. F. Maguire, K. E. Sickafus, *Solid State Ionics*, **140**, 201 (2001).
- [34] J. Chen, J. Lian, L. M. Wang, R. C. Ewing, R. G. Wang, P. W. Pan, *Phys. Rev. Lett.*, **88**, 105901 (2002).
- [35] T. Hagiwara, H. Yamamura, K. Nomura, M. Igawa, *Journal of the Ceramic Society of Japan*, **121**, 205 (2013).
- [36] D. S. Vaisakhan Thampi, P. Prabhakar Rao, A. N. Radhakrishnan, *RSC Advances*, **4**, 12321 (2014).
- [37] J. Singh, A. T. Kalghatgi, J. Parui, S. B. Krupanidhi, *J. Appl. Phys.*, **108**, 054106 (2010).

---

\*Corresponding author: mshakir@ksu.edu.sa